PCCP

Accepted Manuscript

ROYAL SOCIETY OF CHEMISTRY

www.rsc.org/pccp

Trigonal Cu_2-II-Sn-VI_4 (II=Ba, Sr and VI=S, Se) Quaternary Compounds for Earth-Abundant Photovoltaics

Feng Hong,[†,‡] Wenjun Lin,[†] Weiwei Meng,[‡,§] and Yanfa Yan*[‡]*

[†]Department of Physics, Shanghai University, Shanghai 200444, China

[‡]Department of Physics and Astronomy, and Wright Center for Photovoltaic Innovation and Commercialization, The University of Toledo, Toledo, Ohio 43606, USA

[§]School of Physics and Technology, Center for Electron Microscopy, MOE Key Laboratory of Artificial Micro- and Nano-structures, and Institute for Advanced Studies, Wuhan University, Wuhan 430072, China

ABSTRACT: We propose trigonal Cu_2-II-Sn-VI_4 (II=Ba, Sr and VI =S, Se) quaternary compounds for earth-abundant solar cell applications. Through density-functional theory calculations we show that these compounds exhibit similar electronic and optical properties of kesterite Cu_2ZnSnS_4 (CZTS): high optical absorption with band gaps suitable for efficient single-junction solar cell applications. However, the trigonal Cu_2-II-Sn-VI_4 compounds exhibit defect properties more suitable for photovoltaic applications than CZTS. In CZTS, the dominant defects are the deep acceptors, Cu substitutions on Zn sites, which cause non-radiative recombination and limit the open-circuit voltages of CZTS solar cells. On the contrary, the dominant defects are

the shallow acceptors, Cu vacancies, in trigonal Cu_2-II-Sn-VI_4, similar to that in $CuInSe_2$. Our results suggest that the trigonal Cu_2-II-Sn-VI_4 quaternary compounds could be promising candidates for efficient earth-abundant thin-film solar cell and photoeletrochemical water splitting applications.

INTRODUCTION

Solar photovoltaic (PV) is highly desirable for clean, renewable electricity generation. Thin-film PV materials such as Cu(In,Ga)Se_2 (CIGS) and CdTe have demonstrated the viability for clean renewable energy generation.[1-10] Although these technologies are being commercialized, they face some uncertainties with respect to large-scale production due to supply limitations for In, Ga, and Te. Kesterite (KS) Cu_2ZnSnS_4 (CZTS) and $Cu_2ZnSnSe_4$ (CZTSe),[11-20] and their alloys do not contain scarce elements and have been considered potential replacements for the chalcopyrite CIGS absorber, because kesterites and chalcopyrites have similar crystal structures. The kesterite structure is obtained by replacing every two group-III atoms in the chalcopyrite with a group-II and a group-IV atom. However, while CIGS solar cells have achieved a record efficiency of 21.7%,[9] the record efficiency of kesterite solar cell has been only about 12%,[13] significantly lower than the theoretical efficiency limit for kesterite solar cell. The low efficiency for kesterite solar cells is mainly due to the large open-circuit voltage (V_{OC}) deficit, defined as $Eg/q - V_{OC}$, where Eg is the band gap of the absorber and q is the electron charge. For CZTS cells, the V_{OC} deficit can be as large as more than 650 mV,[14-16] comparing to a typical value of 500 mV for CIGS cells.[6] Theoretical studies have revealed the origins for the low V_{OC} deficient for CIGS solar cells.[21] It is know that the V_{OC} is mainly limited by the non-radiation recombination caused by defects in the absorbers and interfaces. CIGS consists of Cu d^{10}

element, which introduces antibonding coupling with Se *p* orbital, raising the valence band maximum (VBM), which consequently makes Cu vacancy (V_{Cu}) a very shallow acceptor. Furthermore, the Cu *d*-Se *p* anti-bonding nature favors the formation of Cu vacancy, making it the dominant defect in CIGS. CZTS also consists of Cu d^{10} element and the V_{Cu} is also a shallow acceptor. However, Cu substitution on Zn (Cu_{Zn}) is a deep acceptor and it exhibits a lower formation energy than V_{Cu}, due to the small size mismatch between Cu^{1+} (0.91Å) and Zn^{2+} (0.88 Å) ions and similar structural environment for Cu and Zn.[22] Zn^{2+} and Sn^{4+} (0.83 Å) also have very small size mismatch, leading to easy formation of cation anti-site defects, Zn on Sn (Zn_{Sn}) or Sn on Zn (Sn_{Zn}). Therefore, CZTS is expected to exhibit more non-radiative recombination than CIGS. Furthermore, kesterite CZTS contains three cation elements with the same coordination, resulting in the formation of a large number of defects and defect clusters, leading to high density of tail states and potential fluctuation. As a result, CZTS solar cells have been experiencing large V_{OC} deficits. A legitimate approach to solve this issue is to replace Zn with another group-II element that has large size mismatch with Cu, such as Be, Ca, Sr, and Ba. A recent paper has studied the stability of all possible substitution design[23,24] for kesterite compounds.[25] A series of quaternary I_2-II-IV-VI_4 compounds have been proposed, with I = Cu, Ag, II = Mg, Ca, Sr, Ba, Zn, Cd, IV = Si, Ge, Sn, Pb, Ti, Zr, Hf, and VI = O, S, Se, Te.[25-35] It was found that the cation substitution using elements with large size mismatch leads to large lattice distortion and make the kesterite structure unstable. For example, Cu_2BaSnS_4, Ag_2BaSnS_4, and Cu_2SrSnS_4 have been synthesized.[28-30] Instead of kesterite, these quaternary compounds exhibit a trigonal crystal structure with space group $P3_1$. Though Ba^{2+} (1.49 Å) and Sr^{2+} (1.32 Å) have large size mismatch with Cu^{1+} (0.91 Å) and Sn^{4+} (0.83 Å), these compounds have not attracted any attention possibly simply because they are not kesterites.

In this paper, we investigate the stability and electronic, optical, and defect properties of Cu_2-II-Sn-VI_4 quaternary compounds with a trigonal crystal structure by density-functional theory (DFT) calculations. Our results show that trigonal Cu_2-II-Sn-VI_4 compounds have similar electronic and optical properties with CZTS. However, these trigonal quaternary compounds exhibit defect properties that are more suitable for photovoltaic applications than CZTS: the dominant defects are the shallow acceptors in trigonal Cu_2-II-Sn-VI_4, similar to that seen in $CuInSe_2$. Our results suggest that the trigonal Cu_2-II-Sn-VI_4 quaternary compounds could be promising candidates for efficient earth-abundant thin-film solar cell and photoelectrochemical water splitting (PEC) applications.

CALCULATION METHODS

The DFT calculations were performed using the projector-augmented wave (PAW) method[36,37] implemented in Vienna *ab initio* simulation package (VASP).[38] The cutoff energy for the plane-wave basis set was 400 eV. The generalized gradient approximation (GGA) of Perdew-Burke-Ernzerhof (PBE),[39] and the screened hybrid Heyd-Scuseria-Ernzerhof (HSE)[40,41] functionals were used for exchange-correlation. The HSE functional consists of 25% exact Hartree-Fock exchange mixed with 75% PBE exchange. All atoms were relaxed until the Hellmann-Feynman forces on them were smaller than 0.01 eV/Å. A 8 × 8 × 2 *k*-point mesh was used for structure optimization and electronic properties calculations, and a 16 × 16 × 4 *k*-point mesh was employed in optical absorption calculations. Γ-point-only calculation with a (3 × 3 × 2) host supercell (432 atoms) was adopted to study the defect properties. For defect calculations, we have performed GGA+U calculations by considering on-site Coulomb interaction (U) on Cu 3*d* (8.5 eV) and Sn 4*d* (5.5 eV) orbitals. HSE was not used for defect calculation due to high computational demanding.

RESULTS AND DISCUSSION

Structural properties: The experimentally synthesized quaternary compounds Cu_2BaSnS_4 and Cu_2SrSnS_4, exhibit a trigonal crystal structure with space group $P3_1$ (see Figure 1),[28-30] in which each Cu and Sn is tetrahedrally surrounded by sulfur ions. Two Cu-derived and one Sn-derived tetrahedrons share a corner and thus each sulfur atom is three-fold coordinated with two Cu and one Sn. Group-II atoms (Ba, Sr) are located at the interstitial sites in the tetrahedral framework, forming rows along the [100] and [010] directions.

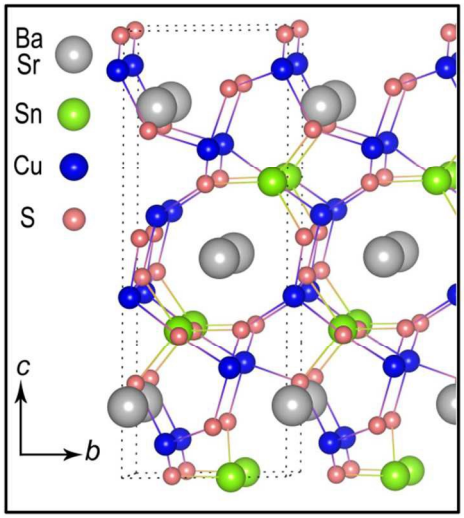

Figure 1. The atomic structure of Cu_2-II-SnS_4 (II = Ba, Sr) with the $P3_1$ phase.

The optimized lattice parameters and band gaps calculated using GGA and HSE functionals are listed in Table 1. For comparison, the calculated results for kesterite structure were also given, though it was predicted thermodynamically unstable by previous and our own theoretical calculations. It can be seen from Table 1 that GGA and HSE calculations slightly overestimate the lattice constants, whereas GGA+U calculation well reproduces the lattice constants of the experimental values.[28,30] It should be pointed out that Cu_2BaSnS_4 and Cu_2SrSnS_4 with the trigonal $P3_1$ phase are more stable than the kesterite structure. In Ref. 25, the authors supposed

that the instability of kesterite structure of these compounds is due to the formation of binary (BaS, SrS) and ternary ($BaSnS_3$ and $SrSnS_3$) compounds. If these secondary phases have non-tetrahedral configurations as in kesterite structure, the quaternary compounds tend to separation. Following this rule, either Ba or Sr atoms prefer non-tetrahedral coordinates for $Cu_2Ba(Sr)SnS_4$ with $P3_1$ structure, therefore the trigonal phase is more stable than the kesterite structure.

Table 1. Calculated lattice parameters (*a*, *c*), band gaps (Eg) and formation enthalpy (ΔH) for the Cu_2BaSnS_4 and Cu_2SrSnS_4 with $P3_1$ and kesterite structure. U = 8.5 eV for Cu 3*d* and 5.5 eV for Sn 4*d* orbital are used for GGA+U calculations.

		Lattice constant (Å)				E_g (eV)			ΔH (eV)	
	Phase	PBE	GGA+U	HSE	Exp.[28,30]	PBE	GGA+U	HSE	PBE	GGA+U
	$P3_1$	*a*=6.450, *c*=15.867	*a*=6.393, *c*=15.852	*a*=6.410, *c*=15.862	a=6.367, c=15.833	0.38	1.62	1.79	-6.50	-7.70
Cu_2BaSnS_4	KS	*a*=5.880, *c*=11.580	*a*=11.604	-	-	0.19	1.12	-	-5.24	-6.33
	$P3_1$	*a*=6.360 *c*=15.624	*a*=6.297, *c*=15.586	*a*=6.318, *c*=15.617	*a*=6.290, c=15.578	0.39	1.60	1.78	-6.28	-7.50
Cu_2SrSnS_4	KS	*a*=5.723, *c*=11.712	*a*=5.686, *c*=11.721	-	-	0.31	1.39	-	-5.51	-6.61

Thermodynamic stability: To investigate whether or not secondary phases may form, we have investigated the thermodynamic stability of Cu_2BaSnS_4 with the trigonal $P3_1$ structure using GGA+U calculations. Under thermodynamic equilibrium growth conditions, to form Cu_2BaSnS_4, the chemical potentials of host elements should satisfy[42,43]

$$2\mu_{Cu} + \mu_{Ba} + \mu_{Sn} + 4\mu_{S} = \Delta H(Cu_2BaSnS_4) = -7.70 \text{ eV} \quad (1)$$

where μ_i is the chemical potential of the constitute element referred to its most stable phase and $\Delta H(Cu_2BaSnS_4)$ is the formation enthalpy of Cu_2BaSnS_4. To avoid the formation of possible secondary phases such as binary CuS, Cu_2S, BaS, SnS, and SnS_2, and ternary such as Cu_2SnS_3 and $BaSnS_3$ compounds, the following constraints must also be satisfied:

$$\mu_{Cu} + \mu_{S} < \Delta H(CuS) = -0.58 \text{ eV} \quad (2)$$

$$2\mu_{Cu} + \mu_{S} < \Delta H(Cu_2S) = -1.01 \text{ eV} \quad (3)$$

$$\mu_{Ba} + \mu_{S} < \Delta H(BaS) = -4.17 \text{ eV} \quad (4)$$

$$\mu_{Sn} + \mu_{S} < \Delta H(SnS) = -1.02 \text{ eV} \quad (5)$$

$$\mu_{Sn} + 2\mu_{S} < \Delta H(SnS_2) = -1.78 \text{ eV} \quad (6)$$

$$2\mu_{Cu} + \mu_{Sn} + 3\mu_{S} = \Delta H(Cu_2SnS_3) = -3.08 \text{ eV} \quad (7)$$

$$\mu_{Ba} + \mu_{Sn} + 3\mu_{S} = \Delta H(BaSnS_3) = -6.07 \text{ eV} \quad (8)$$

Under these constraints, a chemical region in three dimensional μ_{Cu}, μ_{Ba}, and μ_{Sn} chemical space was found, suggesting that the trigonal $P3_1$ phase is thermodynamically stable without the formation of secondary phases in this chemical region. We have done similar calculations for Cu_2BaSnS_4 with the kesterite structure, but no chemical region was found for stable Cu_2BaSnS_4 without the formation of secondary phases, in agreement with previous calculations.[25] The stable region for trigonal $P3_1$ Cu_2BaSnS_4 in different μ_{Cu} planes (μ_{Cu}=0, -0.2, -0.58 and -0.815 eV) were shown in Figures 2. Under Cu-rich growth condition (such as μ_{Cu}=-0.2 eV, see Figure 2(b)), the chemical range of Sn is mainly determined by the formation of SnS and Cu_2S. It should be pointed out that GGA calculation also predicted the thermodynamic stability of $P3_1$ structure, in

which the μ_{Sn} range is mainly confined by the formation of SnS and CuS under Cu-rich condition, which is similar to the case of CZTS.[22,44,45]

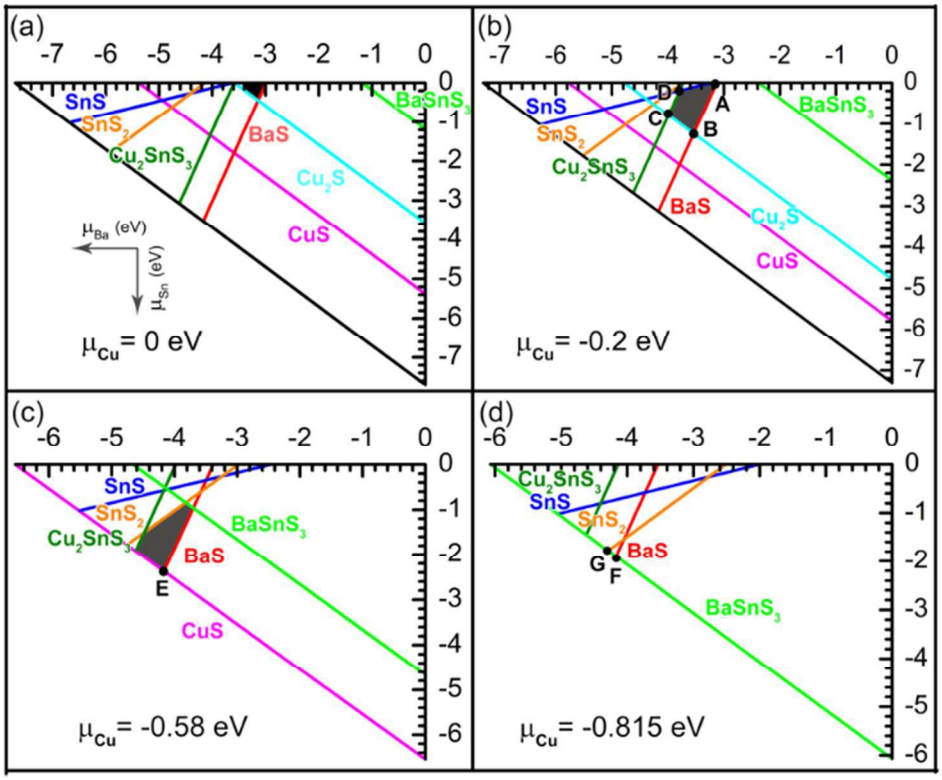

Figure 2. Chemical range for thermodynamically stable Cu_2BaSnS_4 $P3_1$ structure spanned by Ba and Sn chemical potentials in different μ_{Cu} planes.

The difference is attributed to the significant underestimation of the formation enthalpy for Cu_2S by GGA calculation. Our GGA calculation shows a difference of 0.01 eV for the formation enthalpy between Cu_2S and CuS, in accordance with previous calculations (0.03 eV[45] and 0 eV[46]), whereas it is considerably smaller than that calculated using GGA+U (-0.43 eV, present work) and HSE (-0.35 eV[46]), as well as experimental value (-0.27 eV[47]). Therefore, GGA+U calculations give more reliable results than GGA calculations. Hence, only GGA+U results are discussed in this paper.

A stable chemical range was also found for Cu_2SrSnS_4 with the $P3_1$ structure (see Figure S1(b)). However, the chemical potential window is much smaller than that for Cu_2BaSnS_4 due to the lower formation enthalpy of Cu_2SrSnS_4 (-7.50 eV) and higher formation enthalpy of SrS (-4.30 eV). Therefore stable range confined by the formation of Cu_2SnS_3 and SrS is narrower. Nonetheless, our calculations indicate that Cu_2BaSnS_4 and Cu_2SrSnS_4 with the trigonal $P3_1$ phase are thermodynamically stable, in agreement with experimental results.[28-30]

Electronic properties: The HSE calculated band structures and partial density of states (PDOS) for Cu_2BaSnS_4 (Cu_2SrSnS_4) with $P3_1$ structure are shown in Figures 3 (a)-(d). It is seen that Cu_2BaSnS_4 (Cu_2SrSnS_4) exhibits an indirect band gap of 1.77 (1.77) eV. The conduction band minimum (CBM) is at Γ-point, whereas the VBM is near Γ point along the Γ-A line. Importantly, however, the difference between the direct band gap at Γ-point, 1.79 (1.78) eV, and the indirect band gap is only 0.02 (0.01) eV. This slight difference does not affect the optical absorption. Similar to CZTS, the VBM of Cu_2BaSnS_4 (Cu_2SrSnS_4) is composed of antibonding states from Cu 3*d* and S 3*p*, while the CBM is mainly derived from Sn 5*s* with a small component of S 3*p* and 3*s* states. Ba (Sr) does not make significant contribution to the VBM edge (see Figure 3(b) and (d)), partially due to the strong ionic characteristics. Both conduction and valence bands are as dispersive as that of CZTS (Figure S2), suggesting that the electron and hole masses of these quaternary phases are expected to be similar to that of CZTS. The electron and hole masses are expected to be similar to that of CZTS. Cu and Sn maintain the tetrahedral environment in Cu_2BaSnS_4 (Cu_2SrSnS_4) as they do in CZTS. Therefore, Cu_2BaSnS_4 and Cu_2SrSnS_4 should exhibit similar optical properties of CZTS.

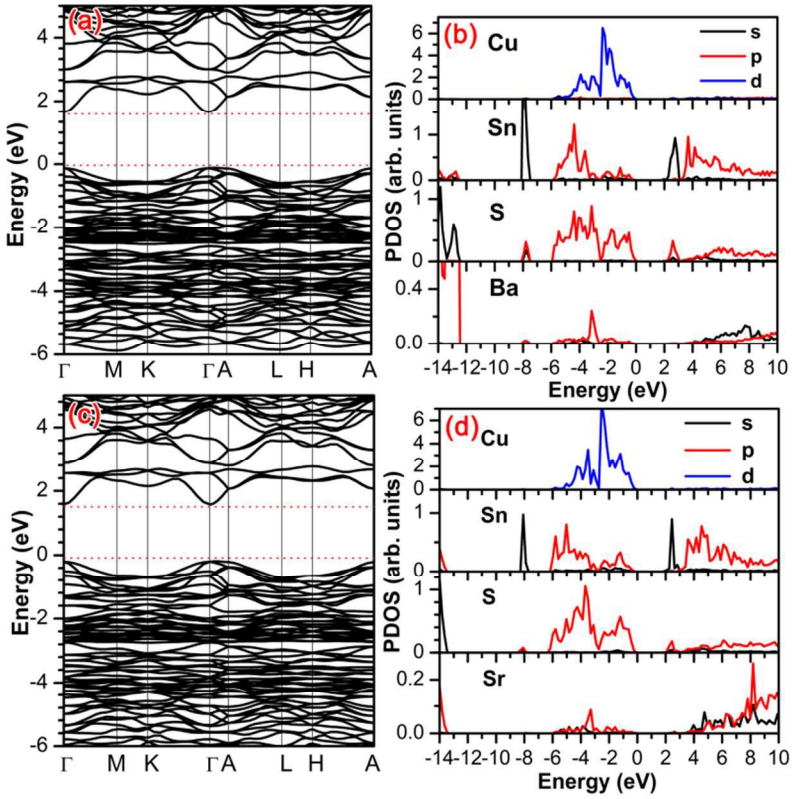

Figure 3. The HSE calculated (a) and (c) band structures, and (b) and (d) PDOS for Cu_2BaSnS_4 and Cu_2SrSnS_4 with $P3_1$ structure, respectively.

Optical properties: The band gaps of 1.77 eV of Cu_2BaSnS_4 and Cu_2SrSnS_4 is slightly larger than the optimal band gap (1.1-1.5 eV) for efficient single junction solar cell application from the Schockly-Queisser limit.[48] However, the band gap can be tuned down by alloying with Se, an isovalent element to S. This is because the Se 4*p* is higher in energy than S 3*p*, so the alloying with Se will push up the VBM. Meanwhile, Se 4*p*-Sn 5*s* hybridization is weaker than S 4*p*-Sn 5*s* due to the larger Se-Sn bond length. Therefore, the alloying with Se will shift down the CBM slightly. This alloying approach has been successfully used to lower the band gap of CZTS.

We have calculated the band gaps of $Cu_2BaSnS_{4-x}Se_x$ with various x using HSE, and found that the band gap decreases monotonically with the increase of x value, as shown in Figure 4(a). The calculated band gap is 1.28 eV for $Cu_2BaSnSe_4$. The alloying with Se is not expected to reduce the optical absorption. The calculated GGA+U optical absorption coefficients of $Cu_2BaSnS_{4-x}Se_x$ alloys (x = 0, 1, 2, 3, and 4) and CZTS are shown in Figure 4(b). The method used for the calculation can be found elsewhere.[49-51] As the VASP code with HSE give unrealistic tails in the calculated optical absorption coefficient, we used GGA+U calculation. The U parameters were carefully determined so that the GGA+U calculated band gap for each composition matches with the band gap predicted by HSE calculation.

It is seen that $Cu_2BaSnS_{4-x}Se_x$ alloys exhibit similar absorption feature as CZTS, except for different onset energies (band gaps). We have also calculated the maximum efficiencies[49-51] of these alloys as function of thickness using the calculated absorption coefficients, shown in Figure 4(c). As expected, the conversion efficiency of Cu_2BaSnS_4 is lower than that of CZTS at all thicknesses, due to its larger band gap. The $Cu_2BaSnS_2Se_2$ shows efficiencies comparable with CZTS, due to the reduced band gap. For clarity, the HSE calculated band structures for $Cu_2BaSnSe_4$ and $Cu_2SrSnSe_4$ are also plotted in Figure S3. From literature survey, there have been no reports on experimental synthesis of $Cu_2BaSnSe_4$ and $Cu_2SrSnSe_4$. To see whether or not $Cu_2BaSnSe_4$ is stable to be synthesized, we have also studied the thermodynamic stability for $Cu_2BaSnSe_4$. The results are shown in Figure S1(c). It is seen that a chemical potential window for stabilizing this compound dose exist, indicating that this compound is also thermodynamically stable. Since no chemical window was found for stable $Cu_2SrSnSe_4$ without the formation of secondary phases (see Figure S1(d), the concentration of Se should be carefully controlled when synthesize $Cu_2SrSn_{4-x}Se_x$.

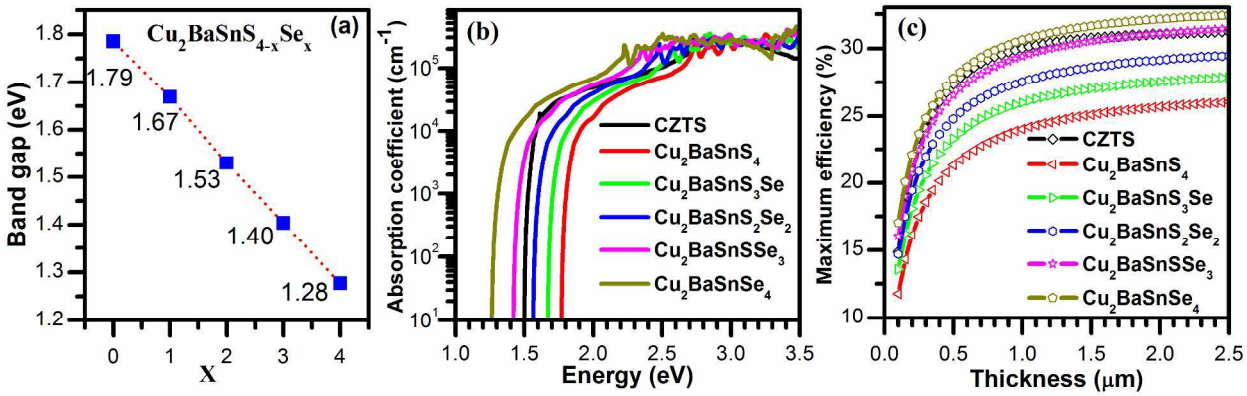

Figure 4. (a) HSE calculated band gap of $Cu_2BaSnS_{4-x}Se_x$, (b) calculated optical absorption coefficients, (c) maximum efficiencies as a function of thickness for $Cu_2BaSnS_{4-x}Se_x$ and CZTS.

Defect properties: The photovoltaic properties of a solar cell depend on the defect properties of the absorber such as transition energy levels and formation energies of point defects. We have calculated the transition energy levels and formation energies of point defects in Cu_2BaSnS_4 using the standard method.[42,43,52] Because GGA calculations significantly underestimate the bandgap of Cu_2BaSnS_4, we used GGA+U (8.5 eV for Cu 3*d* and 5.5 eV for Sn 4*d* orbital) to avoid large errors.

All possible point defects were considered in our calculations, including four vacancies (V_{Cu}, V_{Ba}, V_{Sn}, V_S), four interstitials (Cu_i, Ba_i, Sn_i, S_i), six cation substitutions (Cu_{Ba}, Cu_{Sn}, Ba_{Cu}, Ba_{Sn}, Sn_{Cu}, Sn_{Ba},), and six cation on anion and anion on cation antisite substitutions (Cu_S, Ba_S, Sn_S, S_{Cu}, S_{Ba}, S_{Sn}). We have tested four sites for each interstitial and considered the most stable configuration. It was found that Cu_i favors a site tetrahedrally surrounded by four S atoms, whereas Ba_i, Sn_i, S_i prefer the bridge site in the Ba row.

The calculated transition energy levels for acceptor-like and donor-like defects are shown in Figures 5(a) and (b), respectively. It is seen that V_{Cu} and Cu_{Ba} are shallow acceptors, whereas Cu_i

and Ba_{Cu} are shallow donors. All other defects produce deeper levels in the band gap. V_{Cu} is a shallow acceptor in both Cu_2BaSnS_4 and CZTS. This is because their valence bands have the same nature, comprising of Cu *d*-S *p* antibonding states.[22,44,45,53] Due to the strong ionic characteristic, Cu_2BaSnS_4 have more shallow defects than CZTS. For example, while Cu_{Zn} is a deeper acceptor (~0.1 eV) than V_{Cu} in CZTS,[44] the Cu_{Ba} is still shallow (~0.01 eV higher than V_{Cu}) in Cu_2BaSnS_4. Furthermore, Ba is rather ionic, making Ba related defects such as vacancies and interstitials also shallow, resembling the situation of CH_3NH_3 related defects in $CH_3NH_3PbI_3$ perovskite.[54-56]

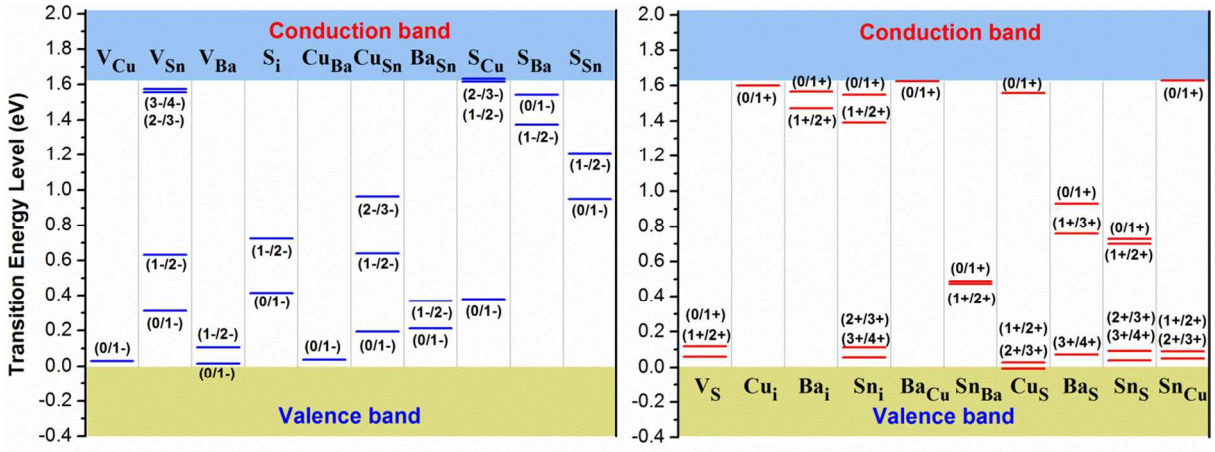

Figure 5. Calculated transition energy levels of (a) acceptor-like and (b) donor-like intrinsic defects in Cu_2BaSnS_4.

It should be pointed out that these U values (8.5 eV for Cu 3*d* and 5.5 eV for Sn 4*d* orbital) predict a band gap of 1.62 eV, which is still smaller than the band gap of 1.78 eV predicted by HSE. We find that it is not necessary to use unrealistically large U values to calculate defect properties. We have calculated defect levels using different U parameters, such as U = 6 eV for Cu 3*d* orbital, and found that the shallow levels such as, V_{Cu}, Cu_i, Cu_{Ba} and Ba_{Cu}, do not change significantly (see Figure S4).

The deeper level of Cu_{Zn} in CZTS can be understood by considering that the Cu on Zn antisite enhances the *p–d* hybridization, so the corresponding energy level of Cu_{Zn} is pushed up, and thus exhibits a deeper level than that of V_{Cu}.[22,45] In Cu_2BaSnS_4, the *p-d* hybridization induced by Cu_{Ba} is weak due to its long Cu-S bond length. Thus, the acceptor level of Cu_{Ba} is not much deeper than that of V_{Cu}. The shallow nature of donors Cu_i and Ba_{Cu} can be understood by the fact that Cu 4*s* and Ba 5*s* states have higher energy levels than Sn 5*s*, and thus have little influence on the bottom of conduction bands. Furthermore, V_{Ba} levels in Cu_2BaSnS_4 are not as deep as V_{Zn} levels in CZTS.

As the photovoltaic properties are determined by the dominant defects present in the absorber, we have calculated the formation energies of all considered point defects. As the formation energies depend on the chemical potentials (growth conditions) of the constituent elements,[45,57] we have chosen the following seven chemical potentials points, A-D (Cu-rich/S-poor), and E-G (Cu-poor/S-rich) (see Figure 2), to calculate the formation energies of neutral defects.

Figure 6 shows the calculated formation energies as a function of chemical potentials. For clarity, the defects that have formation energy higher than 2.5 eV at all chemical potentials points are not shown. The four defects that create shallow levels are indicated by the solid lines, whereas the rest are indicated by dotted lines. It is seen that V_{Cu} and Cu_i have lower formation energies than Cu_{Ba} and Ba_{Cu}. In contrast, Cu_{Zn} is always the dominant defect in CZTS. This is largely due to the fact that Cu^{1+} and Ba^{2+} have large size mismatch, but Cu^{1+} and Zn^{2+} have small size mismatch. At chemical potential range A-D (Cu-rich/S-poor), the dominant defects are V_{Cu}, Cu_i, and V_S, among which only V_{Cu} and Cu_i are shallow defect. V_S is a deep donor, and therefore is detrimental to solar cell performance. At chemical potential range E-F (Cu-poor/S-rich), the

dominant defect is always the shallow acceptor, V_{Cu}, similar to the situation in $CuInSe_2$, indicating that Cu_2BaSnS_4 films grown under these conditions should exhibit good photovoltaic properties. The formation energies are also dependent on the Fermi levels for charged defects. We have therefore calculated the formation energies of all-above considered defects with various charge states as a function of Fermi level position at two representative points A (Cu-rich/S-poor) and F (Cu-poor/S-rich), as shown in Figure 7. It is seen that the conductivity of Cu_2BaSnS_4 depends on the growth conditions. At chemical potential point A (see Figure 7(a)), the Fermi level is pinned at 0.84 eV above VMB by V_{Cu} and Cu_i. Therefore Cu_2BaSnS_4 synthesized at this growth condition should be either intrinsic or slightly *n*-type. At chemical potential point F (see Figure 7(b)), the Fermi level is determined by V_{Cu} and Cu_i, which is only 0.22 eV above the VBM, indicating that Cu_2BaSnS_4 grown under this condition should exhibit excellent *p*-type conductivity, which resembles the widely observed intrinsic *p*-type conductivity in CZTS.[11,58-60]

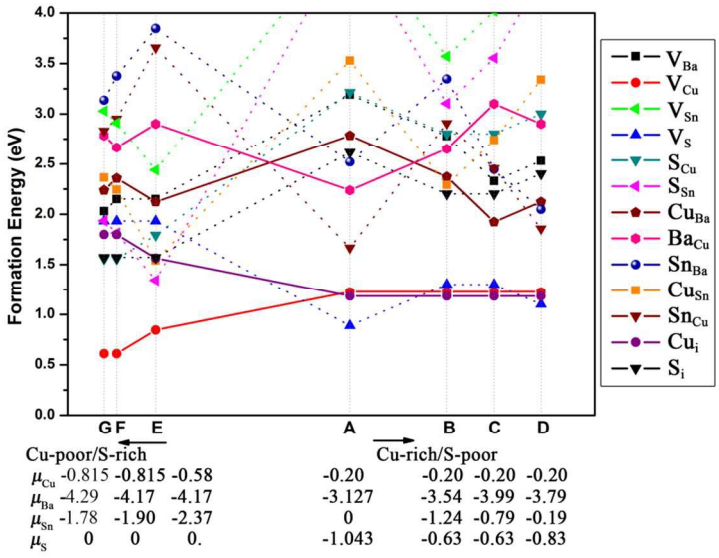

Figure 6. Calculated formation energies of intrinsic charge neutral defects as a function of chemical potentials.

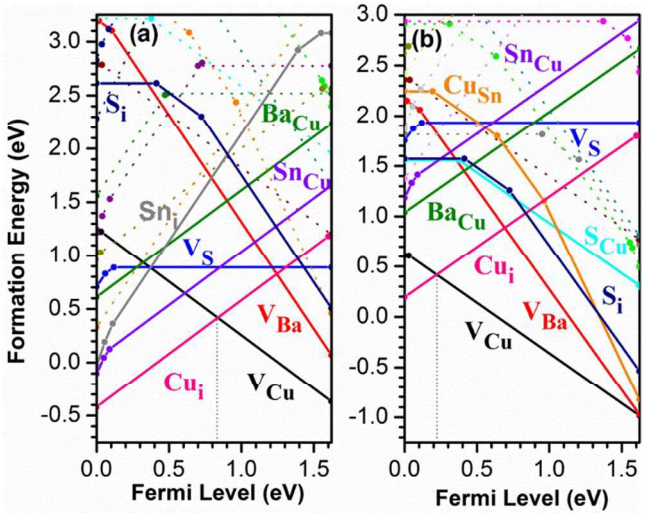

Figure 7. Calculated formation energies of intrinsic point defects as a function of the Fermi level at point A (a) and point F (b). The vertical dotted line indicates the Fermi level pinning

CONCLUSION

In conclusion, we show by density-functional theory calculations that the trigonal c Cu_2-II-Sn-VI_4 (II=Ba, Sr and VI =S, Se) quaternary compounds are attractive candidate for earth-abundant solar cell and PEC water splitting applications. Like CZTS, these compounds exhibit high optical absorption with band gaps suitable for efficient single-junction solar cell applications. Importantly, we find that these trigonal quaternary compounds exhibit defect properties that are more suitable for photovoltaic applications than CZTS. In CZTS, the dominant defect is deep acceptor, Cu_{Zn}, due to small size mismatch between Cu^+ and Zn^{2+}. However, Ba^{2+} and Sr^{2+} have large size mismatch with and different coordination than Cu^{1+} and Sn^{4+} in trigonal Cu_2-II-Sn-VI_4 (II=Ba, Sr and VI =S, Se) quaternary compounds, making the shallow acceptor V_{Cu} the dominant defect, which is similar to the situation in CIGS. Other deep level cation on cation anti-site defects such as Ba or Sr on Cu or Sn (Ba_{Cu}, Ba_{Sn}, Sr_{Cu}, Sr_{Sn}) do not form easily due to the trigonal structure. Our results strongly suggest that the trigonal Cu_2-II-

Sn-VI_4 (II=Ba, Sr and VI =S, Se) quaternary compounds are promising candidates as replacements of CZTS for efficient earth-abundant thin-film solar cell and PEC applications.

ASSOCIATED CONTENT

Supporting Information. This material is available free of charge via the Internet at http://pubs.acs.org.

AUTHOR INFORMATION

Corresponding Author

* E-mail: fenghong@shu.edu.cn. * E-mail: yanfa.yan@utoledo.edu.

ACKNOWLEDGMENT

The work was supported by the National Science Foundation under contract no. CHE-1230246, CBET-1433401, and DMR-1534686 and Natural Science Foundation of China (Grant No. 11104177). This research also used the resources of high performance computing platform of Shanghai University, the Ohio Supercomputer Center and the National Energy Research Scientific Computing Center, which is supported by the Office of Science of the U.S. Department of Energy under Contract No. DE-AC02-05CH11231.

REFERENCES

1 W. Witte, D. Abou-Ras, K. Albe, G. H. Bauer, F. Bertram, C. Boit, R. Brüggemann, J. Christen, J. Dietrich, A. Eicke, D. Hariskos, M. Maiberg, R. Mainz, M. Meessen, M. Muller, O. Neumann, T. Orgis, S. Paetel, J. Pohl, H. Rodriguez-Alvarez, R. Scheer, H. W. Schock, T. Unold, A. Weber and M. Powalla, *Prog. Photovoltaics*, 2015, **23**, 717-733.

2 H. W. Schock and R. Noufi, *Prog. Photovoltaics*, 2000, **8**, 151-160.

3 S. Siebentritt, *Sol. Energ. Mat. Sol. C.*, 2011, **95**, 1471-1476.

4 Y. K. Liao, M. Brossard, D. H. Hsieh, T. N. Lin, M. D. B. Charlton, S. J. Cheng, C. H. Chen, J. L. Shen, L. T. Cheng, T. P. Hsieh, F. I. Lai, S. Y. Kuo, H. C. Kuo, P. G. Savvidis and P. G. Lagoudakis, *Adv. Energy Mater.*, 2015, **5**, 1401280.

5 T. J. Jacobsson, V. Fjällström, M. Edoff and T. Edvinsson, *Sol. Energ. Mat. Sol. C.*, 2015, **134**, 185-193.

6 S. Niki, M. Contreras, I. Repins, M. Powalla, K. Kushiya, S. Ishizuka and K. Matsubara, *Prog. Photovoltaics*, 2010, **18**, 453-466.

7 I. Repins, M. A. Contreras, B. Egaas, C. DeHart, J. Scharf, C. L. Perkins, B. To and R. Noufi, *Prog. Photovoltaics*, 2008, **16**, 235-239.

8 P. Jackson, D. Hariskos, E. Lotter, S. Paetel, R. Wuerz, R. Menner, W. Wischmann and M. Powalla, *Prog. Photovoltaics*, 2011, **19**, 894-897.

9 P. Jackson, D. Hariskos, R. Wuerz, O. Kiowski, A. Bauer, T. M. Friedlmeier and M. Powalla, *Phys. Stat. Sol. RRL*, 2015, **9**, 28-31.

10 M. A. Contreras, L. M. Mansfield, B. Egaas, J. Li, M. Romero, R. Noufi, E. Rudiger-Voigt and W. Mannstadt, *Prog. Photovoltaics*, 2012, **20**, 843-850.

11 M. Grossberg, J. Krustok, K. Timmo and M. Altosaar, *Thin Solid Films*, 2009, **517**, 2489-2492.

12 S. Y. Chen, X. G. Gong, A. Walsh and S. H. Wei, *Appl. Phys. Lett.*, 2009, **94**, 041903.

13 W. Wang, M. T. Winkler, O. Gunawan, T. Gokmen, T. K. Todorov, Y. Zhu and D. B. Mitzi, *Adv. Energy Mater.*, 2014, **4**, 1301465.

14 T. K. Todorov, J. Tang, S. Bag, O. Gunawan, T. Gokmen, Y. Zhu and D. B. Mitzi, *Adv. Energy Mater.*, 2013, **3**, 34-38.

15 K. Wang, O. Gunawan, T. Todorov, B. Shin, S. J. Chey, N. A. Bojarczuk, D. Mitzi and S. Guha, *Appl. Phys. Lett.*, 2010, **97**, 143508.

16 D. B. Mitzi, O. Gunawan, T. K. Todorov, K. Wang and S. Guha, *Sol. Energ. Mat. Sol. C.*, 2011, **95**, 1421-1436.

17 K. J. Wang, B. Shin, K. B. Reuter, T. Todorov, D. B. Mitzi and S. Guha, *Appl. Phys. Lett.*, 2011, **98**, 051912.

18 G. Rey, A. Redinger, J. S. Ler, T. P. Weiss, M. Thevenin, M. Guennou, B. El Adib and S. Siebentritt, *Appl. Phys. Lett.,* 2014, **105**, 112106.

19 I. L. Repins, M. J. Romero, J. V. Li, S. H. Wei, D. Kuciauskas, C. S. Jiang, C. Beall, C. DeHart, J. Mann, W. C. Hsu, G. Teeter, A. Goodrich and R. Noufi, *Ieee J. Photovolt.*, 2013, **3**, 439-445.

20 D. B. Mitzi, O. Gunawan, T. K. Todorov and D. A. R. Barkhouse, *Philos. Trans. R. Soc. London, Ser. A*, 2013, **371**, 20110432.

21 S. B. Zhang, S.-H. Wei, A. Zunger and H. Katayama-Yoshida, *Phys. Rev. B*, 1998, **57**, 9642-9656.

22 S. Chen, A. Walsh, X. G. Gong and S. H. Wei, *Adv. Mater*, 2013, **25**, 1522-1539.

23 C. H. L. Goodman, *J. Phys. Chem. Solids*, 1958, **6**, 305-314.

24 B. R. Pamplin, *J. Phys. Chem. Solids*, 1964, **25**, 675-684.

25 C. Wang, S. Chen, J.-H. Yang, L. Lang, H.-J. Xiang, X.-G. Gong, A. Walsh and S.-H. Wei, *Chem. Mater.*, 2014, **26**, 3411-3417.

26 G. M. Ford, Q. Guo, R. Agrawal and H. W. Hillhouse, *Chem. Mater.*, 2011, **23**, 2626-2629.

27 S. Levcenco, D. Dumcenco, Y. S. Huang, K. K. Tiong and C. H. Du, *Opt. Mater.*, 2011, **34**, 183-188.

28 C. L. Teske and O. Vetter, *Z. Anorg. Allg. Chem.*, 1976, **426**, 281-287; C. R. L. Teske and O. Vetter, *Z. Anorg. Allg. Chem.*, 1976, **427**, 200-204; C. L. Teske, *Z. Anorg. Allg. Chem.*, 1976, **419**, 67-76; M. Tampier; D. Johrendt, *Z. Anorg. Allg. Chem.*, 2001, **627**, 312-320.

29 P. A. Hersh, Wide band gap semiconductors and insulators: Synthesis, processing, and characterization. Ph. D. Thesis, Oregon State University, 2008.

30 A. Assoud; N. Soheilnia; H. Kleinke, *Chem. Mater*. 2005, **17**, 2255-2261.

31 O. V. Parasyuk, L. D. Gulay, L. V. Piskach and I. D. Olekseyuk, *J. Alloy. Compd.*, 2002, **335**, 176-180.

32 L. D. Gulay, Y. E. Romanyuk and O. V. Parasyuk, *J. Alloy. Compd.*, 2002, **347**, 193-197.

33 T. Washio, T. Shinji, S. Tajima, T. Fukano, T. Motohiro, K. Jimbo and H. Katagiri, *J. Mater. Chem.*, 2012, **22**, 4021.

34 X. F. Wang, J. J. Li, Z. J. Zhao, S. M. Huang and W. H. Xie, *J. Appl. Phys.*, 2012, **112**, 023701.

35 B. W. Liu, M. J. Zhang, Z. Y. Zhao, H. Y. Zeng, F. K. Zheng, G. C. Guo and J. S. Huang, *J. Solid State Chem.*, 2013, **204**, 251-256.

36 P. E. Blöchl, *Phys. Rev. B*, 1994, **50**, 17953-17979.

37 G. Kresse and D. Joubert, *Phys. Rev. B*, 1999, **59**, 1758-1775.

38 G. Kresse and J. Furthmüller, *Phys. Rev. B*, 1996, **54**, 11169-11186.

39 J. P. Perdew, K. Burke and M. Ernzerhof, *Phys. Rev. Lett.*, 1996, **77**, 3865-3868.

40 J. Heyd, G. E. Scuseria and M. Ernzerhof, *J. Chem. Phys.*, 2003, **118**, 8207-8215.

41 A. V. Krukau, O. A. Vydrov, A. F. Izmaylov, and G. E. Scuseria, *J. Chem. Phys.*, 2006, **125**, 224106.

42 S.-H. Wei, *Comp. Mater. Sci.*, 2004, **30**, 337-348.

43 Y. Yan and S.-H. Wei, *Phys. Status Solidi B,* 2008, **245**, 641-652.

44 S. Y. Chen, X. G. Gong, A. Walsh and S. H. Wei, *Appl. Phys. Lett.*, 2010, **96**, 021902.

45 A. Walsh, S. Y. Chen, S. H. Wei and X. G. Gong, *Adv. Energy Mater.*, 2012, **2**, 400-409.

46 D. Han, Y. Y. Sun, J. Bang, Y. Y. Zhang, H. B. Sun, X. B. Li and S. B. Zhang, *Phys. Rev. B*, 2013, **87**, 155206.

47 F. Macdonald and D. R. Lide, *Pap. Am. Chem. S*, 2003, **225**, U552-U552.

48 W. Shockley and H. J. Queisser, *J. Appl. Phys.*, 1961, **32**, 510-519.

49 L. P. Yu and A. Zunger, *Phys. Rev. Lett.*, 2012, **108**, 068701.

50 L. P. Yu, R. S. Kokenyesi, D. A. Keszler and A. Zunger, *Adv. Energy Mater.*, 2013, **3**, 43-48.

51 W. J. Yin, J. H. Yang, J. Kang, Y. F. Yan and S. H. Wei, *J. Mater. Chem. A*, 2015, **3**, 8926-8942.

52 C. Freysoldt, B. Grabowski, T. Hickel, J. Neugebauer, G. Kresse, A. Janotti and C. G. Van de Walle, *Rev. Mod. Phys.*, 2014, **86**, 253-305.

53 S. H. Wei and S. B. Zhang, *J. Phys. Chem. Solids*, 2005, **66**, 1994-1999.

54 W.-J. Yin, T. Shi and Y. Yan, *Appl. Phys. Lett.*, 2014, **104**, 063903.

55 W. J. Yin, T. Shi and Y. Yan, *Adv. Mater*, 2014, **26**, 4653-4658.

56 W.-J. Yin, T. Shi and Y. Yan, *J. Phys. Chem. C*, 2015, **119**, 5253-5264.

57 G.-X. Qian, R. M. Martin and D. J. Chadi, *Phys. Rev. B*, 1988, **38**, 7649-7663.

58 H. Katagiri, K. Saitoh, T. Washio, H. Shinohara, T. Kurumadani and S. Miyajima, *Sol. Energ. Mat. Sol. C*, 2001, **65**, 141-148.

59 N. Nakayama and K. Ito, *Appl. Surf. Sci.*, 1996, **92**, 171-175.

60 Y. B. K. Kumar, G. S. Babu, P. U. Bhaskar and V. S. Raja, *Sol. Energ Mater. Sol. Cells*, 2009, **93**, 1230-1237.

TOC Graphics